Intermodulation Distortion of a Comb-Based RF Photonic Filter Using Balanced Detection

Hyoung-Jun Kim and Andrew M. Weiner

***Abstract*— We investigate intermodulation distortion of a tunable radio frequency photonic filter utilizing an optical frequency comb, an interferometric configuration, and a balanced detection. When the filter passband is tuned from 2 to 7 GHz, this scheme has the third-order spurious free dynamic range of <108.2 dB·Hz$^{2/3}$. In addition, we investigate the effect of Mach–Zehnder modulator (MZM) configuration on second-order intermodulation. A high extinction ratio MZM results in 43-dB lower power in the second-order intermodulation tones compared with that obtained with a conventional MZM.**

***Index Terms*— Frequency comb, microwave photonics, tunable filters, spurious free dynamic range, intermodulation distortion, balanced detection.**

I. Introduction

In ELECTRONICS, for radio frequency (RF) systems, tunable RF filters using varactor diodes, microelectromechanical systems, Yttrium iron garnet resonators, and active inductors have been used. Recently, photonics-based schemes have also received much attention due to their tunability and programmability over a large RF frequency range. Because of these advantages, RF photonic filtering enables implementation of wideband RF systems requiring multi-functionality and frequency-agility. However, their RF performance has been rarely considered. Compared with analog-optic links, achieving good RF metrics in RF photonic filters is more difficult due to optical losses originating from components required for filter design. In addition, only one optical sideband contributes to RF gain of the tunable filter. Although an optical amplifier can increase RF gain, it also generates optical noise and thus degrades the noise figure. Furthermore, nonlinearities in optical modulators and photodetectors cause intermodulation distortion [1]–[5]. Spurious free dynamic range (SFDR), which is one of the key RF metrics, is limited by intermodulation (IM) effects and output noise. SFDR3 is mainly considered because it is difficult to eliminate the third-order IM tones close to fundamental RF tones. For wideband applications SFDR2 should also be considered since the second-order IM of strong interfering signals far from the passband may cause signal distortion in the filter passband.

Manuscript received June 30, 2015; revised July 29, 2015; accepted August 16, 2015. Date of publication August 20, 2015; date of current version October 2, 2015. This work was supported in part by the Office of the Assistant Secretary of Defense for Research and Engineering within the National Security Science and Engineering Faculty Fellowship Program through the Naval Postgraduate School under Grant N00244-09-1-0068 and in part by the National Research Foundation of Korea within the Basic Science Research Program through the Ministry of Education under Grant NRF-2014R1A6A3A03059647.

The authors are with the School of Electrical and Computer Engineering, Purdue University, West Lafayette, IN 47907 USA (e-mail: sjun27@purdue.edu; amw@purdue.edu).

Color versions of one or more of the figures in this letter are available online at http://ieeexplore.ieee.org.

Digital Object Identifier 10.1109/LPT.2015.2470667

In photonics, RF filtering has been demonstrated via approaches based on linear optical filters [6]–[8], Brillouin-gain resonance [9], [10], and tapped delay lines [11]–[16]. In the optical filtering approach, an RF-modulated optical signal is transmitted to the optical filter and then an RF frequency band can be selected or suppressed. Various optical filter structures with multiple poles or cells have been integrated in a semiconductor substrate (e.g. silicon or InP) [6]–[8]. However, high optical loss of the filter chip limits SFDR3 to <104.1 dB·Hz$^{2/3}$ [8]. The dynamic range of filters based on Brillouin gain has not been reported to the best of our knowledge [9], [10]. The tapped delay line approach is based on a finite impulse response and can be implemented with a multiple wavelength source and single dispersive fiber [11]–[16]. A scheme using two laser-diodes and two fiber Bragg gratings achieved SFDR3 of 106.05 dB·Hz$^{2/3}$ [13]. However, other RF metrics such as RF gain and noise figure were poor. In addition, the filter passband characteristic was limited by two filter taps. In previous work of our group, the use of an optical frequency comb enabled to scale to a large number of filter taps over 100 [14] and to achieve extremely rapid tuning (tens of nanoseconds) [15]. Recently, we improved the RF gain and noise figure of the comb-based scheme by introducing an interferometric configuration and balanced detection [16]. However, the SFDR characteristics of these comb-based filters have not been investigated yet.

Various linearization techniques have been extensively investigated to suppress the third-order intermodulation distortion in analog optic links [1]. For example, a phase-modulated link using parallel interferometric demodulation achieved the SFDR of up to 131 dB (1 Hz bandwidth) [2]. In [11], a tapped delay line filtering scheme using a spectrally sliced optical noise source employed a linearization technique using polarization-sensitive modulation in a LiNbO3 phase modulator and the dispersion-induced linear/nonlinear phase-to-intensity conversion [11]. In this work, the third-order intermodulation distortion was significantly suppressed. However, the total output noise was still high due to the incoherent noise source used and limits the dynamic range.

In this letter, we investigate intermodulation distortion of a tunable RF photonic filter using an optical frequency comb in an interferometric configuration with balanced detection. Our scheme achieved the highest SFDR3 (<108.2 dB·Hz$^{2/3}$) among photonics-based filtering schemes, preserving other RF metric performance and filtering characteristics. The SFDR3 variation from 2 to 7 GHz is < 1.2 dB. The second-order distortion is also important for wideband applications and thus has been extensively investigated in analog-optic links [1]. However, it has not been investigated for RF photonic filtering, except for [12]. In [12], an incoherent broadband light source spectrally sliced by a Mach-Zehnder interferometer enabled a single filter passband. Suppression of second-order

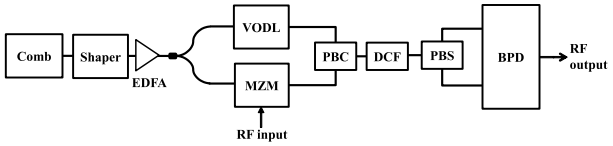

Fig. 1. Filter configuration. (PBC/PBS: polatization beam combiner/splitter, VODL: variable optical delay line).

harmonics generated outside of the filter passband by ∼30dB was reported. Here we examine the more critical situation where the second-order intermodulation tone (IM2) occurs within the filter passband. We report measurements in which the use of a balanced Mach-Zehnder modulator (MZM) results in 43 dB lower IM2 power compared to that obtained with a conventional MZM.

II. RF Photonic Filter

Fig. 1 shows the configuration of the RF photonic filter. The optical frequency comb is carved by the programmable pulse shaper to control filter amplitude taps, amplified by the erbium-doped fiber amplifier (EDFA) to increase the output photocurrent, and directed to the interferometer. The interferometer has a variable optical delay line in one arm and a MZM biased at the minimum transmission point in the other. The outputs of the variable optical delay line and MZM are connected to a polarization beam combiner. The polarization- multiplexed signals are directed to a polarization beam splitter through a dispersion compensating fiber (DCF) where dispersion introduces linear differential tap delay. The outputs of the polarization beam splitter are connected to the balanced photodetector (BPD). The single DCF with polarization multiplexing is used to balance two complementary signal paths for balanced detection. The filter transfer function can be expressed by [16]

$$H(\omega_{RF}) \propto \sum_{n}^{N} P_n \left[e^{j[n\Delta\omega(\psi_2\omega_{RF}\pm\tau)]} \right] \tag{1}$$

where P_n is the power of n^{th} optical comb lines; $\Delta\omega$ is the comb spacing; ψ_2 is the second-order phase coefficient of the DCF; ω_{RF} is the RF frequency; τ is the relative delay difference between the two interferometer arms. Equation (1) indicates a Fourier transformation relationship between the shapes of the optical frequency comb and the filter passband. Because of this relationship, various filter passbands can be implemented by programming the pulse shaper. In addition, the filter center frequency is tunable by changing the interferometer delay difference through the variable optical delay line.

There are several design considerations to improve RF performance [16]. Firstly, to enhance RF gain, the EDFA is used to increase output photocurrent. Secondly, the MZM and balanced detection suppress the intensity noise originating from the EDFA. Finally, the use of asymmetric input interferometer split ratio optimizes the interferometer path loss ratio related to the power difference between the optical carrier and sideband. It maximizes RF gain at a fixed photocurrent and thus minimizes noise figure. The principle of our scheme is similar to low-biased links [3], [16].

The third order intermodulation distortion (IMD3) is defined as the ratio of the third order intermodulation tone (IM3) power to the fundamental tone power at the filter output. When photodetector nonlinearity is negligible, the IMD3 caused by the nonlinear transfer curve of the MZM is given by [4]

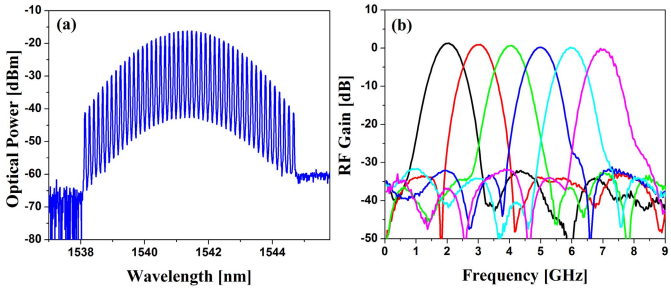

Fig. 2. (a) Spectra of Gaussian-shaped comb with resolution of 0.05 nm and (b) frequency tuning of the filter passband.

$$IMD3 = \left(\frac{J_2(\beta)J_1(\beta)}{J_1(\beta)J_0(\beta)} \right)^2 \tag{2}$$

where $\beta = \pi V_{RF}/V_\pi$; V_{RF} is the voltage amplitude of each of the two-tones (assumed equal); V_π is the half-wave voltage of the MZM. The IM tones generated by the MZM are affected by the same filter response function seen by the fundamental tones because the delay difference between fundamental tones and IM tones is negligible. As a result, out-of-band IM tones can be suppressed by the filter. In addition, the balanced detection suppresses common mode IM tones caused by beating between optical tones from the MZM.

Unlike low-biased analog-optic links which suffer from second-order distortion, our scheme can provide good RF gain and noise figure as well as significant suppression of the even-order distortion by the use of a well-balanced MZM with high extinction ratio. This is achieved by biasing at minimum transmission for carrier-suppressed modulation for which even order distortion is suppressed [5].

III. Experiment

A nearly flat optical frequency comb with 18 GHz repetition rate is generated by cascaded intensity and phase modulation of a continuous-wave laser. Fig. 2(a) shows the spectrum of a Gaussian-shaped comb at the output of the pulse shaper (Finisar WaveShaper 1000S/SP). The number of comb lines is 47, corresponding to the number of filter taps. We use two different MZMs. MZM1 is a z-cut modulator (EOSPACE AZ-0K5-10) with half-wave voltage of 3V@1GHz and extinction ratio of 20 dB. MZM2 is an x-cut modulator (EOSPACE AX-6K5-10) with symmetric electrode configuration and half-wave voltage of 3.6V@1GHz. MZM2 incorporates an integrated polarizer and an extra electrode for precisely balancing its two arms, yielding a higher extinction ratio (∼30 dB). The DCF provides a dispersion of −400 ps/nm, resulting in differential tap delay of 57.1 ps. The BPD (Discovery Semiconductors DSC720-HLPD) has responsivity of 0.65 A/W.

In a first set of experiments, we use MZM1 and split ratio of 10:90 at the input to the interferometer (90% of the power directed to the MZM). Fig. 2(b) shows frequency tuning of the filter passband in the range of 2 to 7 GHz. The RF gain is nearly 0 dB. The 3-dB filter bandwidth and stopband attenuation are 700 MHz and >30 dB, respectively. To account for the internal matching resistor of the BPD, 6 dB is added to the power measured at the BPD output [16].

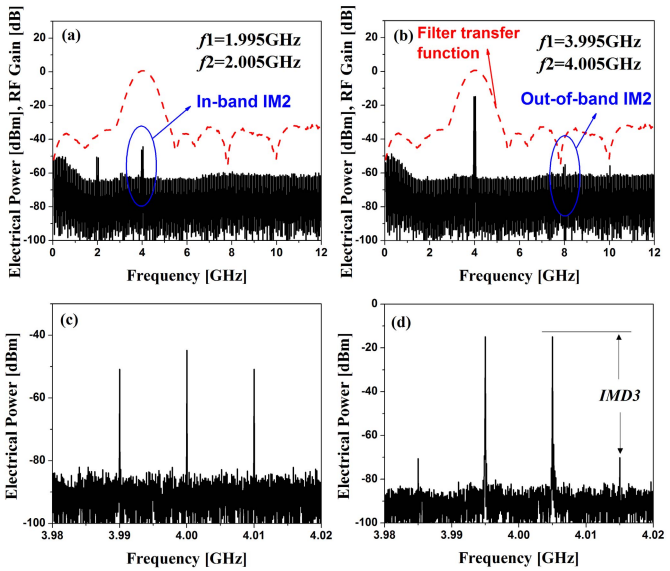

Fig. 3. RF spectra with a filter transfer function at the BPD output for different two-tone center frequencies of (a) 2 GHz and (b) 4 GHz (resolution=3MHz); (c) and (d) shows zoom-in spectra of in-band IM2 and IM3, respectively (resolution=470kHz). $f1$ and $f2$ are two-tone frequencies.

We perform two-tone tests to investigate effects of the second- and third-order nonlinearities on IM2 and IM3, respectively. Fig. 3(a) and (b) show the same filter transfer function with 4 GHz filter center frequency (f_{filter}). Fig. 3(a) and (b) also show RF spectra at the BPD output for two center frequencies of two-tones ($f1$ and $f2$). The two-tone frequency spacing is 10 MHz. The power of each input tone is -15dBm. When the two-tone center frequency ($f_{\text{two-tone}}$) is half of the filter center frequency ($f_{\text{two-tone}} = f_{\text{filter}}/2$), as shown in Fig. 3(a), the fundamental tones (1.995 and 2.005 GHz) and IM3 (1.985 and 2.015 GHz) are out of filter passband and suppressed by the filter transfer function. However, as shown in Fig.3(c), the IM2 at 4 GHz is generated in the filter passband. It means that strong interfering signals at $f_{\text{filter}}/2$ cause serious signal distortion in the filter passband due to the second-order nonlinearity of the filter. This important effect in filtering schemes was not previously reported to our knowledge. As shown in Fig. 3(b) and (d), when the center frequencies of the two-tones and the filter are 4GHz, the IM3 at 3.985 and 4.015GHz are generated in the filter passband. Compared to the in-band IM2 power at 4 GHz, the out-of-band IM2 power at 8 GHz is suppressed by only $\sim$10 dB. The suppression is lower than the filter stopband attenuation ($>$30 dB) due to photodetector nonlinearity. At 10 GHz, a tone is observed outside one Nyquist zone due to the beating of the comb line and the second-order optical sideband.

Fig. 4 shows the IMD3 and output photocurrent as a function of the EDFA output power. The center frequencies of the two-tones and the filter are 4GHz. The power of each input tone is set to 0 dBm. As the EDFA output power increases, the photocurrent is increased. According to (2), when the MZM nonlinearity is dominant, the IMD3 is independent of the output photocurrent. In other words, the power of fundamental tone and IM3 increase with the same slope when photodiode nonlinearity is negligible. Below an EDFA power of 16 dBm, the measured IMD3 agrees with the modulator-limited value (-38.2 dBc) calculated by (2). However, as the EDFA

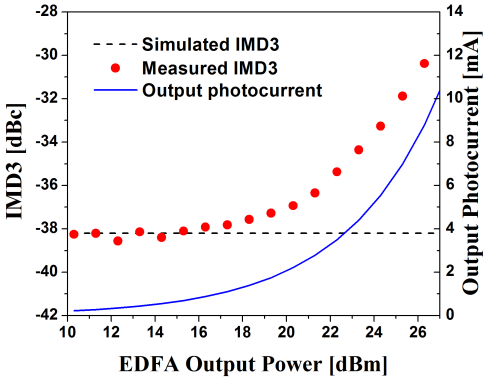

Fig. 4. IMD3 and output photocurrent as a function of the EDFA output power.

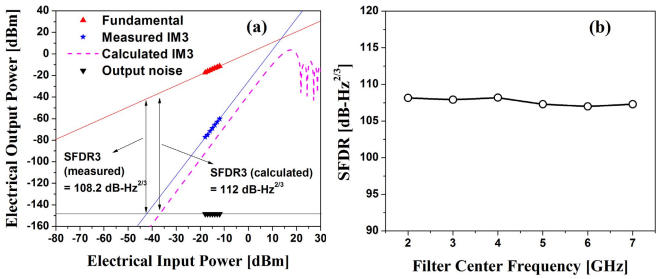

Fig. 5. (a) SFDR3 curve and (b) SFDR3 with respect to filter center frequencies.

power further increases, the measured value increases above the value calculated on the basis of modulator nonlinearity alone. Above 21 dBm EDFA power, the measured IMD3 increases with a slope of $\sim$1. This indicates that due to nonlinear mixing at the BPD, the IM3 power increases much faster with higher photocurrents than the fundamental power. Fig. 5(a) shows a SFDR3 curve at 19.7 mA photocurrent when the center frequencies of the two-tones and the filter are both 4GHz. As the fundamental power increases, the output IM3 power increases with a slope of 3. The peak RF gain at 4 GHz is 0.67 dB and output measured noise is -148.4 dBm/Hz. It results in a noise figure of 25 dB. The measured SFDR3 is 108.2 dB$\cdot$Hz$^{2/3}$, which is $\sim$4 dB lower than the modulator-limited value (112 dB$\cdot$Hz$^{2/3}$) calculated from (2). This is a consequence of photodetector nonlinearity. When the filter passband is tuned from 2 to 7 GHz, the SFDR3 varies by only 1.2 dB (Fig. 5(b)).

The effects of the MZM extinction ratio, limited by intensity and phase imbalance of the two MZM arms, on in-band IM2 are investigated when the two-tone center frequency is half of the filter center frequency ($f_{\text{two-tone}} = f_{\text{filter}}/2$). In this experiment, the in-band IM2 using modulators MZM1 and MZM2 is compared. The optical power handling of MZM2 (13 dBm) is much lower than that of MZM1 (30 dBm). The maximum achievable RF gain with MZM2 is much lower than that with MZM1 due to its lower optical power handling and higher half-wave voltage. For the measurement with MZM2, we used a 50:50 input split ratio to the interferometer to increase the RF gain. To have the same peak RF gain of -23.4 dB, MZM1 and MZM2 are used with photocurrents of 1.2 and 6.2 mA, respectively. Based on data similar to that of Fig. 3(c), the IM2 power at 4 GHz is measured with increasing power of the input two-tones. Fig.6 shows in-band IM2 with MZM1 and MZM2. As the input power of the fundamental tones increases,

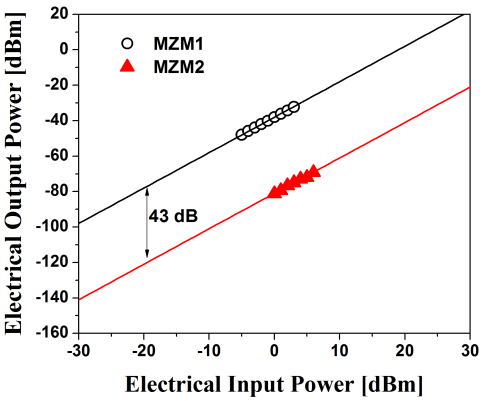

Fig. 6. In-band IM2 output power for MZM1 and MZM2 cases.

TABLE I

RF PERFORMANCE COMPARISON OF TUNABLE FILTERING SCHEMES

Schemes		RF gain [dB]	NF [dB]	SFDR3 [dB·Hz$^{2/3}$]
Varactor diode [17]		0	14	110
Active inductor [18]		4.7	25.6	98
Integrated optical filtering	Silicon [6]*	1.7	54	94.3
	InP [7]	-	23.2	86.3
	Silicon [8]*	10	36	104.1
Dispersive -tapped delay line	Incoherent noise source [11]	-51.2	92	-
	Two LDs [13]	-25	40	106.05
	Frequency comb [This work]	0.67	25	108.2

* Both RF filtering and down-conversion were performed.
NF: noise figure; LD: laser diode.

the output power of the IM2 is increased with a slope of 2. Due to its higher extinction ratio, the experiment with MZM2 results in 43 dB lower IM2 compared to that with MZM1.

Typical microwave applications requires SFDR3 values of 105∼120 dB·Hz$^{2/3}$ [7]. As shown in Table 1, representative SFDR3's of potentially rapidly tunable electronic filtering schemes are 98 and 110 dB·Hz$^{2/3}$, respectively, limited by high noise and nonlinearity of the varactor diode and active inductor tuning elements [17], [18]. A commercial preselector including varactor filters and low-noise-amplifiers has the SFDR3 of 105 dB·Hz$^{2/3}$ [19]. Recently, low-biased analog-optic links achieved an SFDR3 of ∼120 dB·Hz$^{2/3}$ [3]. Despite disadvantages such as higher optical loss compared to links, our filtering scheme yields SFDR3 up to 108.2 dB·Hz$^{2/3}$, already competitive with varactor and active inductor based tunable filters. The adoption of higher linearity BPDs [1] or linearization techniques [2] could further reduce the IM3 power. In addition, the use of a MZM with a higher extinction ratio should enable shot noise-limited performance [16]. If IMD3 and output noise are limited by the MZM and by shot noise, respectively, we estimate that an SFDR3 up to 117 dB·Hz$^{2/3}$should be possible at ∼20 mA photocurrent, similar to what was used here.

IV. CONCLUSION

We investigate intermodulation distortion of a tunable RF photonic filter using an optical frequency comb, interferometric configuration, and balanced detection. It provides a SFDR3 of <108.2 dB·Hz$^{2/3}$ without degradation of filter characteristics, RF gain, and noise figure. The SFDR3 variation is less than 1.2 dB for filter frequency tuning from 2 to 7 GHz. Furthermore, we have shown that IM2 can be substantially suppressed by using a high extinction ratio modulator. The results suggest that our scheme can be used in frequency-agile RF applications.

REFERENCES

[1] V. J. Urick, J. F. Diehl, M. N. Draa, J. D. McKinney, and K. J. Williams, "Wideband analog photonic links: Some performance limits and considerations for multi-octave implementations," *Proc. SPIE*, vol. 8259, pp. 82590401–82590414, Feb. 2012.

[2] J. D. McKinney, K. Colladay, and K. J. Williams, "Linearization of phase-modulated analog optical links employing interferometric demodulation," *J. Lightw. Technol.*, vol. 27, no. 9, pp. 1212–1220, May 1, 2009.

[3] H. V. Roussell *et al.*, "Gain, noise figure and bandwidth-limited dynamic range of a low-biased external modulation link," in *Proc. IEEE Int. Topic Meeting Microw. Photon.*, Victoria, BC, Canada, Oct. 2007, pp. 84–87.

[4] B. H. Kolner and D. W. Dolfi, "Intermodulation distortion and compression in an integrated electrooptic modulator," *Appl. Opt.*, vol. 26, no. 17, pp. 3676–3680, Sep. 1987.

[5] C.-T. Lin, J. J. Chen, S.-P. Dai, P.-C. Peng, and S. Chi, "Impact of nonlinear transfer function and imperfect splitting ratio of MZM on optical up-conversion employing double sideband with carrier suppression modulation," *J. Lightw. Technol.*, vol. 26, no. 15, pp. 2449–2459, Aug. 1, 2008.

[6] K.-Y. Tu *et al.*, "Silicon RF-photonic filter and down-converter," *J. Lightw. Technol.*, vol. 28, no. 20, pp. 3019–3028, Oct. 15, 2010.

[7] E. J. Norberg, R. S. Guzzon, J. S. Parker, L. A. Johansson, and L. A. Coldren, "Programmable photonic microwave filters monolithically integrated in InP–InGaAsP," *J. Lightw. Technol.*, vol. 29, no. 11, pp. 1611–1619, Jun. 1, 2011.

[8] H. Yu, M. Chen, P. Li, S. Yang, H. Chen, and S. Xie, "Silicon-on-insulator narrow-passband filter based on cascaded MZIs incorporating enhanced FSR for downconverting analog photonic links," *Opt. Exp.*, vol. 21, no. 6, pp. 6749–6755, 2013.

[9] B. Vidal, M. A. Piqueras, and J. Martí, "Tunable and reconfigurable photonic microwave filter based on stimulated Brillouin scattering," *Opt. Lett.*, vol. 32, no. 1, pp. 23–25, 2007.

[10] W. Zhang and R. A. Minasian, "Widely tunable single-passband microwave photonic filter based on stimulated Brillouin scattering," *IEEE Photon. Technol. Lett.*, vol. 23, no. 23, pp. 1775–1777, Dec. 1, 2011.

[11] X. Xue, X. Zheng, H. Zhang, and B. Zhou, "Spectrum-sliced microwave photonic filter with an improved dynamic range based on a $LiNbO_3$ phase modulator and balanced detection," *IEEE Photon. Technol. Lett.*, vol. 24, no. 9, pp. 775–777, May 1, 2012.

[12] M. Rius, J. Mora, M. Bolea, and J. Capmany, "Harmonic distortion in microwave photonic filters," *Opt. Exp.*, vol. 20, no. 8, pp. 8871–8876, 2012.

[13] Y. Yan and J. Yao, "Photonic microwave bandpass filter with improved dynamic range," *Opt. Lett.*, vol. 33, no. 15, pp. 1756–1758, Aug. 2008.

[14] M. Song, V. Torres-Company, R. Wu, A. J. Metcalf, and A. M. Weiner, "Compression of ultra-long microwave pulses using programmable microwave photonic phase filtering with >100 complex-coefficient taps," *Opt. Exp.*, vol. 22, no. 6, pp. 6329–6338, 2014.

[15] V. R. Supradeepa *et al.*, "Comb-based radiofrequency photonic filters with rapid tunability and high selectivity," *Nature Photon.*, vol. 6, pp. 186–194, Feb. 2012.

[16] H.-J. Kim, D. E. Leaird, A. J. Metcalf, and A. M. Weiner, "Comb-based RF photonic filters based on interferometric configuration and balanced detection," *J. Lightw. Technol.*, vol. 32, no. 20, pp. 3478–3488, Oct. 15, 2014.

[17] H. Trabelsi and C. Cruchon, "A varactor-tuned active microwave bandpass filter," *IEEE Microw. Guided Wave Lett.*, vol. 2, no. 6, pp. 231–232, Jun. 1992.

[18] H. Xiao and R. Schaumann, "A 5.4-GHz high-Q tunable active-inductor bandpass filter in standard digital CMOS technology," *Analog Integr. Circuits Signal Process.*, vol. 51, no. 1, pp. 1–9, 2007.

[19] *Specification for NuWaves' High Performance Wideband RF Tuner*. [Online]. Available: http://www.nuwaves.com/wp-content/uploads/2011/03/HiPerTuner-Specification.pdf, accessed Aug. 17, 2015.